REACTION CROSS SECTIONS FOR $^{13-15}$B AND ONE-NEUTRON HALO IN ^{14}B*

M. Tanaka[a], M. Fukuda[a], D. Nishimura[b], M. Takechi[c]
S. Suzuki[d], H. Du[a], Y. Tanaka[a], K. Aoki[b], S. Fukuda[e]
A. Honma[c], T. Izumikawa[f], Y. Kamisho[a], N. Kanda[c], I. Kato[g]
Y. Kanke[b], A. Kitagawa[e], J. Kohno[g], M. Machida[b], K. Matsuta[a]
M. Mihara[a], E. Miyata[c], Y. Morita[a], J. Muraoka[b], D. Murooka[c]
T. Nagai[b], M. Nagashima[c], K. Ohnishi[a], J. Ohno[a], T. Ohtsubo[c]
H. Oikawa[b], S. Sato[e], H. Shimamura[b], T. Sugihara[a], T. Suzuki[g]
N. Tadano[g], R. Takagaki[b], Y. Takei[b], A. Takenouchi[b], S. Yagi[a]
T. Yamaguchi[g], S. Yamaki[g], S. Yamaoka[a]

[a]Department of Physics, Osaka University, Osaka 560-0043, Japan
[b]Department of Physics, Tokyo University of Science, Chiba 278-8510, Japan
[c]Department of Physics, Niigata University, Niigata 950-2102, Japan
[d]Department of Physics, Tsukuba University, Ibaraki 305-8577, Japan
[e]National Institute of Radiological Sciences, Chiba 263-8555, Japan
[f]RI Center, Niigata University, Niigata 951-8510, Japan
[g]Department of Physics, Saitama University, Saitama 338-3570, Japan

(Received December 14, 2016)

We have measured reaction cross sections ($\sigma_{\rm R}$) for ^{13,14,15}B on Be, C, Al, and proton targets. In addition to the conventional method of deducing nucleon density distributions based on the Glauber-type calculation, the recently developed method for deducing point-proton and neutron density distributions separately from $\sigma_{\rm R}$ on proton targets were utilized for these nuclei. The result suggests the necessity for ^{14}B of a large tail in its neutron density distribution, which can be referred to as a one-neutron halo. Root-mean-square point-proton, neutron and matter radii for ^{13,14,15}B were also derived. From present systematic studies for ^{13,14,15}B, a large enhancement of matter and neutron radii in ^{14}B was found for the first time.

DOI:10.5506/APhysPolB.48.461

1. Introduction

The reaction cross-section ($\sigma_{\rm R}$) measurements at intermediate energies have been used to deduce matter densities based on the Glauber-type cal-

* Presented at the Zakopane Conference on Nuclear Physics "Extremes of the Nuclear Landscape", Zakopane, Poland, August 28–September 4, 2016.

culation. This method is a powerful tool to study the surface structure of nuclei, which takes an advantage of the high sensitivity of σ_{R} to low densities at intermediate energies. We have deduced nucleon density distributions of some exotic light nuclides and have clarified those distinctive structures such as proton and neutron halos by this method [1].

It is quite important to discuss point-proton and neutron density distributions respectively for understanding halo and skin structures in detail. Recently, we have developed the new method for the separation of point-proton and neutron density distributions by utilizing the proton–neutron asymmetry of nucleon–nucleon total cross sections in the intermediate energy region [2, 3]. In this method, we employed proton targets as proton–neutron asymmetric targets in addition to conventional nuclear targets. Proton targets are the most appropriate ones for the asymmetric targets because they are the most proton–neutron asymmetric targets. In the present work, we study nuclear structures of neutron-rich boron isotopes ^{13,14,15}B by this method.

For ^{14}B, some experimental studies were performed so far. The magnetic dipole and the electric quadrupole moments for ^{14}B were measured by Okuno *et al.* [4] and by Izumi *et al.* [5], respectively. One-neutron ($1n$) knockout/absorption reactions [6–9] were also measured and these results support a large contribution of $2s_{1/2}$ orbital in a valence neutron configuration though the valence neutron is sitting in $1d_{5/2}$ orbital in a naive shell model. Moreover, a $1n$ separation energy (S_{1n}) of ^{14}B is very small: $S_{1n} = 0.970(21)$ MeV [10]. Therefore, ^{14}B is one of the candidates for the $1n$-halo nucleus. On the other hand, interaction cross sections (σ_{I}) for ^{14}B at relativistic energy are not so large in comparison with neighboring nuclei, ^{13}B and ^{15}B [11]. Furthermore, σ_{R} for ^{14}B at intermediate energy [12] has a large uncertainty. Hence, ^{14}B has not been concluded as a $1n$-halo nucleus through reaction and interaction cross-section measurement prior to the present study.

2. Experiments

We carried out experiments using the HIMAC heavy-ion synchrotron and the SB2 fragment-separator facility at the National Institute of Radiological Sciences (NIRS), Japan [13]. We produced ^{13,14,15}B secondary beams of several energies between 50 and 130 MeV/nucleon by the projectile fragmentation with the combination of 200 MeV/nucleon ^{18}O and Be targets for ^{13,15}B and that of 160 MeV/nucleon ^{15}N or ^{18}O and Be targets for ^{14}B. We employed the transmission method to measure σ_{R} with the same procedure as Ref. [14]. The particle identification (PID) before the reaction target was performed by the $B\rho$–TOF–ΔE method, which consists of HIMAC SB2 fragment-separator and thin plastic counters at the first and the third fo-

cal planes. After the reaction target, the PID was done by using a ΔE–E counter telescope, which consists of several Si and CsI(Tl) ΔE detectors and a NaI(Tl) E detector.

We employed Be, C and Al targets as p–n symmetric reaction targets and a polyethylene (CH_2) target as a p–n asymmetric target. σ_R on a proton target (σ_R^H) was derived by the subtraction of σ_R on a C target (σ_R^C) from σ_R on a CH_2 target ($\sigma_R^{CH_2}$) as $\sigma_R^H = (\sigma_R^{CH_2} - \sigma_R^C)/2$.

3. Results and discussions

Figure 1 shows the present results of σ_R for $^{13,15}B$ by filled symbols as a function of energy together with σ_I at relativistic energy [15]. In order to deduce density distributions from these experimental results, we utilized a fitting procedure with the modified Glauber calculation [1]. In this method, we can deduce the density distribution by adjusting some free parameters in a model function. It is already confirmed that this calculation can reproduce $\sigma_R(E)$ for various nuclides in a wide energy range by taking into account the effects of multiple scattering, the finite range of nuclear force and Fermi motion in the nucleus [14].

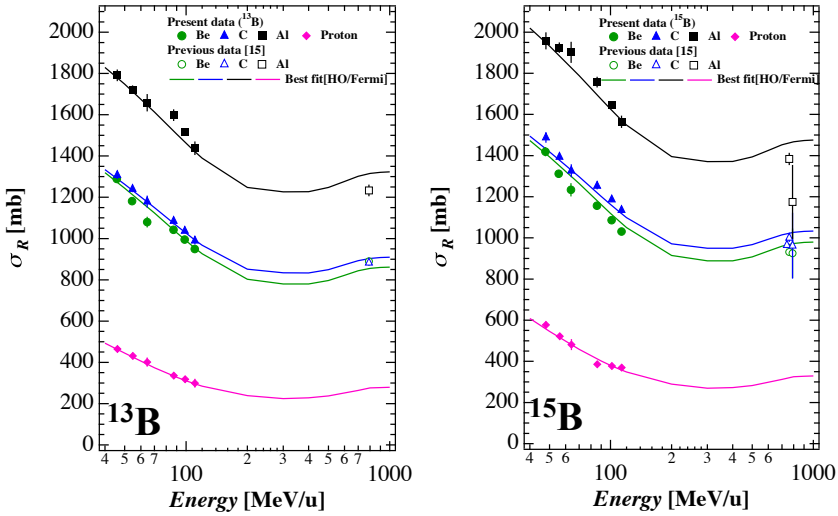

Fig. 1. (Color online) Present experimental $\sigma_R(E)$ for $^{13,15}B$ on Be (circle/green), C (triangle/blue), Al (square/black), and proton (diamond/pink) targets with filled symbols. σ_I at relativistic energy are also shown with empty symbols [15].

First, we deduced nucleon density distributions $\rho_N(r)$ from experimental σ_R on nuclear targets. A Harmonic-Oscillator-type (HO) and Fermi-type function were used as model densities. A χ^2 fitting was performed with

changing the width of the model function as a free parameter. Next, point-proton and neutron density distributions ($\rho_p(r)$ and $\rho_n(r)$), were deduced separately from the experimental $\sigma_{\rm R}^{\rm H}(E)$ with the obtained nucleon densities as described above. We assumed an HO-type function as $\rho_p(r)$ and performed a χ^2 fitting with the width of $\rho_p(r)$ as a free parameter. The solid lines in Fig. 1 show the best-fit results, and corresponding $\rho_N(r)$ and $\rho_p(r)$ are shown by black and gray/red lines, respectively in Fig. 2.

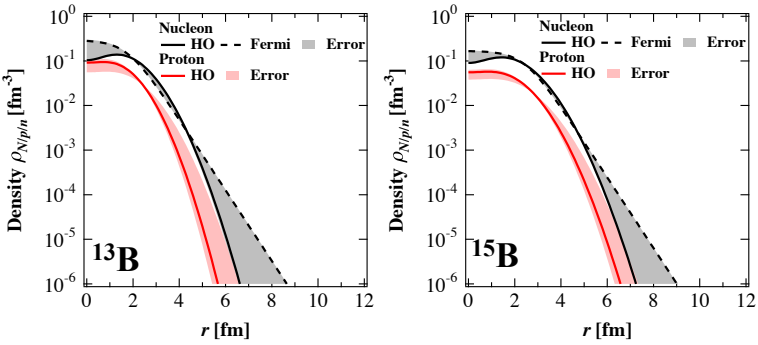

Fig. 2. (Color online) The deduced $\rho_N(r)$ (black) and $\rho_p(r)$ (gray/red) for ^{13,15}B. The solid and dashed lines of nucleon densities are deduced with HO-type and Fermi-type model densities, respectively. Each shaded region represents the error.

The present results of $\sigma_{\rm R}(E)$ for ^{14}B are shown in Fig. 3 (a), (b). In order to deduce density distribution, the same method as the one used for ^{13,15}B was used for ^{14}B. We used not only a HO-type function but also a HO-type plus $1d_{5/2}$ or $2s_{1/2}$ Single-Particle-Model-type (SPM) function as model functions because ^{14}B has mainly two possibilities of valence-neutron configurations indicated by some experiments [4–9]. We performed a χ^2 fitting with the width of HO-type function as a free parameter. The SPM-type density was calculated with the Woods–Saxon potential reproducing the experimental S_{1n} of ^{14}B. In Fig. 3 (a), (b), the best-fit results with above assumptions are shown. Only the HO-type plus $2s_{1/2}$ SPM-type model density can reproduce the energy dependence of the experimental $\sigma_{\rm R}(E)$ very well with $\chi^2/N_{\rm free} = 1.1$. Moreover, when we performed a χ^2 fitting with the width of HO-type function and the number of nucleons in the $2s_{1/2}$ SPM-type density ($N_{\rm SPM}$) as free parameters, $N_{\rm SPM}$ of the best-fit result is $N_{\rm SPM} = 1.15(20)$, which suggests that ^{14}B might be a ^{13}B core plus one neutron system. The deduced $\rho_N(r)$ of ^{14}B is shown in Fig. 3 (c). In the same way as ^{13,15}B, $\rho_p(r)$ and $\rho_n(r)$ of ^{14}B were deduced successfully from $\sigma_{\rm R}^{\rm H}(E)$. A long tail can be seen in its $\rho_n(r)$. Thus, a long neutron tail is needed to reproduce the experimental $\sigma_{\rm R}(E)$ on both nuclear and proton targets.

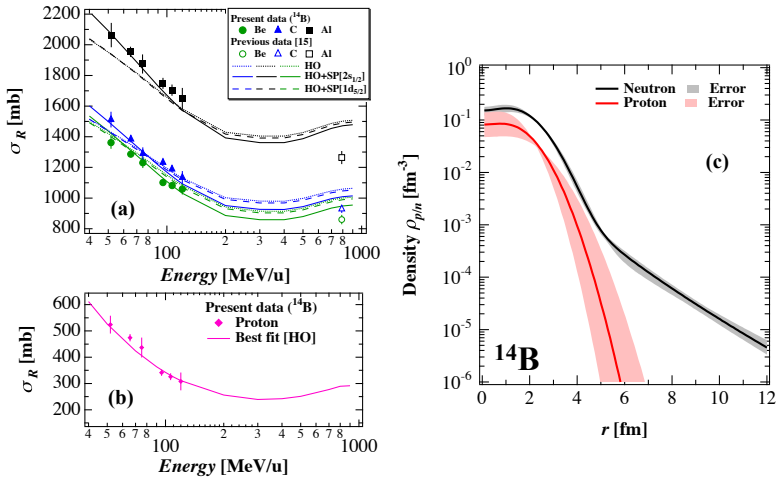

Fig. 3. (Color online) (a), (b) The present experimental $\sigma_{\mathrm{R}}(E)$ for ^{14}B. Each notation means the same as in Fig. 1. The dotted, solid, and dashed lines represent the best-fit results of HO-type, HO-type plus $2s_{1/2}$ SPM-type, and HO-type plus $1d_{5/2}$ SPM-type functions, respectively. (c) The deduced $\rho_N(r)$ (black) and $\rho_p(r)$ (gray/red) for ^{14}B. Each shaded region represents the error.

3.1. Root-mean-square (RMS) radii of B isotopes

RMS radii were derived from the deduced density distributions. Figure 4 shows RMS matter and point-proton radii of neutron rich B isotopes as a

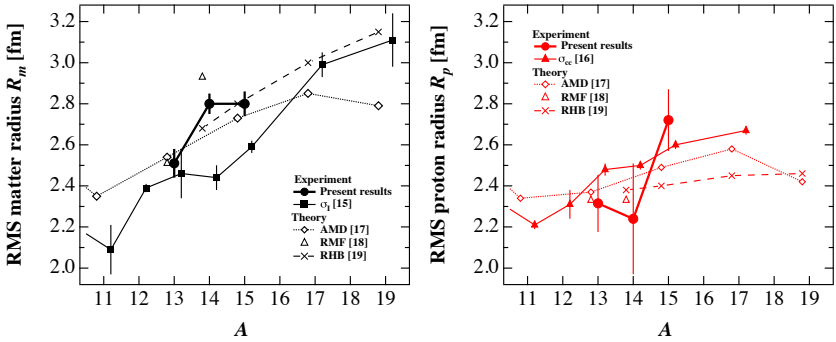

Fig. 4. (Color online) RMS matter (left) and point-proton (right) radii of neutron rich B isotopes as a function of mass number A. Filled circles are present results. Filled squares and triangles are other experimental RMS radii from σ_{I} [15] and σ_{CC} [16], respectively. Empty diamonds, empty triangles, and crosses are theoretical RMS radii of the AMD [17], the Relativistic Mean Field theory [18], and the Relativistic Hartree–Bogoliubov [19] calculations, respectively.

function of mass number A with some experimental [15, 16] and theoretical [17–19] values. Present matter radii of ^{13,15}B are consistent with several theoretical values [17–19]. In addition, the present experimental result shows a large enhancement of the matter radius in ^{14}B, while matter radius deduced from σ_{I} at relativistic energy [15] do not show such an effect. It is considered that the present σ_{R} data are more sensitive to the nuclear surface because of the large nucleon–nucleon total cross sections at intermediate energies. Therefore, this high sensitivity could lead to the first observation of the large matter radius of ^{14}B. On the other hand, though present point-proton radii have relatively large errors, present results are roughly consistent with not only other experimental point-proton radii deduced from σ_{CC} [16] but also theoretical values [17–19].

These experiments of the present work were performed at the NIRS-HIMAC under the research project with heavy ions. The authors are grateful to the staff of HIMAC.

REFERENCES

[1] K. Tanaka *et al.*, *Phys. Rev. C* **82**, 044309 (2010) and references therein.
[2] D. Nishimura *et al.*, *Nucl. Phys. A* **834**, 470c (2010).
[3] T. Moriguchi *et al.*, *Phys. Rev. C* **88**, 024610 (2013).
[4] H. Okuno *et al.*, *Phys. Lett. B* **354**, 41 (1996).
[5] H. Izumi *et al.*, *Phys. Lett. B* **366**, 51 (1996).
[6] D. Bazin *et al.*, *Phys. Rev. C* **57**, 2156 (1998).
[7] V. Guimarães *et al.*, *Phys. Rev. C* **61**, 064609 (2013).
[8] E. Sauvan *et al.*, *Phys. Rev. C* **69**, 044603 (2004).
[9] S. Bedoor *et al.*, *Phys. Rev. C* **88**, 011304(R) (2013).
[10] G. Audi, A.H. Wapstra, *Nucl. Phys. A* **565**, 66 (1993).
[11] I. Tanihata *et al.*, *Phys. Lett. B* **206**, 592 (1988).
[12] A. Ozawa *et al.*, *Nucl. Instrum. Methods Phys. Res. B* **247**, 155 (2006).
[13] M. Kanazawa *et al.*, *Nucl. Phys. A* **746**, 393c (2004).
[14] M. Takechi *et al.*, *Eur. Phys. J. A* **25**, 217 (2005) and references therein.
[15] A. Ozawa *et al.*, *Nucl. Phys. A* **693**, 32 (2001) and references therein.
[16] A. Estradé *et al.*, *Phys. Rev. Lett.* **113**, 132501 (2014).
[17] Y. Kanada-En'yo, *Phys. Rev. C* **91**, 014315 (2015).
[18] Zhongzhou Ren *et al.*, *Z. Phys. A* **357**, 137 (1997).
[19] G.A. Lalazissis *et al.*, *Eur. Phys. J. A* **22**, 37 (2004).